P077 COMMON-REFLECTION-SURFACE STACK AND CONFLICTING DIPS

AUTHOR(S)
J. MANN
Address
Geophysical Institute, University of Karlsruhe, Hertzstr. 16, 76187 Karlsruhe, Germany

Summary. The recently introduced common-reflection-surface (CRS) stack simulates a zero-offset (ZO) section from multi-coverage seismic reflection data for 2-D media in a data-driven way, i. e., without explicit knowledge of the macro-velocity model. The “best” stacking operators are determined by an optimization of the coherency along different test stacking operators in the multi-coverage data. Previous implementations determine only one optimum stacking operator for each ZO sample to be simulated. Consequently, conflicting dips are not taken into account but only the most prominent event contributes to a particular stack sample. In this work, I show how this limitation can be overcome.

The pragmatic search strategy of the original CRS stack implementation consists of three one-parametric search steps to determine the stacking operators. In the first step, an automatic CMP stack, conflicting dips can hardly be considered because the respective stacking velocities might be quite similar. However, I observe that conflicting dips can still be detected and separated in the subsequent search steps that are applied to the result of the automatic CMP stack.

I propose an extension of the pragmatic approach to account for conflicting dips. For ZO samples where conflicting dips are detected, an additional one-parametric search is required. This provides a set of three kinematic wavefield attributes for each of the conflicting events and allows to simulate their interference in the simulated ZO section.

Introduction. The CRS stack method (Müller, 1998, 1999) simulates a ZO section by summing along stacking surfaces in the multi-coverage data. The stacking operator is an approximation of the kinematic reflection response of a curved interface in a laterally inhomogeneous medium. Three kinematic attributes associated with wavefronts of two hypothetical eigenwave experiments are the parameters of the stacking operator. Coherency analyses along various test stacking operators are performed for each particular ZO sample to be simulated. The stacking operator (and its three associated wavefield attributes) yielding the highest coherency is used to perform the actual stack.

However, not only one event might contribute to a particular ZO sample, but different events may intersect at the considered ZO location. To properly simulate a ZO section under such conditions, it is no longer sufficient to consider only one stacking operator for each ZO sample, but separate stacking operators for each contributing event have to be determined. The final stack result can be constructed as a superposition of the contributions of all separate stacking operators.

Pragmatic search strategy. To be able to follow the pragmatic approach of Müller (1998), let me briefly review some theoretical aspects of the CRS stack: I consider the hyperbolic second order representation of the CRS stacking operator (Schleicher et al., 1993; Tygel et al., 1997). Three independent parameters are used to account for the local properties of the subsurface interfaces: the angle of emergence α of the normal ray and the two radii of curvature R_N and R_{NIP} associated with two hypothetical eigenwave experiments (see, e. g., Mann et al., 1999). The stacking operator for a point $P_0 = (x_0, t_0)$ in the ZO section reads

$$t^2\left(x_m, h\right) = \left(t_0 + \frac{2\sin\alpha}{v_0}\left(x_m - x_0\right)\right)^2 + \frac{2\,t_0\cos^2\alpha}{v_0}\left(\frac{\left(x_m - x_0\right)^2}{R_N} + \frac{h^2}{R_{NIP}}\right), \tag{1}$$

where the half-offset between source and receiver is denoted by h, and x_m denotes the midpoint between source and receiver. The only required model parameter is the near surface velocity v_0.
The CRS stack basically consists of a measure of the coherency of the multi-coverage data along all operators given by Equation (1) for any possible combination of values of α, R_{NIP}, and R_N within a specified test range.
In principle, I have to determine the global maximum and a set of local maxima of the coherency measure in the three-parametric attribute domain. However, even the determination of the global maximum turns out to be too time consuming in a three-parametric search strategy. Therefore, I cannot expect to be able to detect additional local maxima in this way.
Müller (1998) proposed to split the three-parametric problem into three one-parametric searches and an optional three-parametric local optimization as depicted in the following simplified flowchart:

$$\begin{array}{ccccc}
 & & \boxed{\text{multi-coverage data}} & & \\
 & & \Downarrow & & \\
 & & \boxed{\text{automatic CMP stack}} & & \\
\Downarrow\ v_{NMO} & & & & \text{ZO section}\Downarrow \\
\boxed{\text{calculate } R_{NIP}} & \overset{\alpha}{\Leftarrow} & & & \boxed{\text{searches for } \alpha \text{ and } R_N} \\
\Downarrow\ R_{NIP} & & & & \alpha \text{ and } R_N\ \Downarrow \\
 & & \boxed{\text{optional optimization and stack with multi-coverage data}} & &
\end{array}$$

The first search step of this pragmatic approach is an automatic CMP stack. The search parameter is the stacking velocity v_{NMO} which can be written in terms of the CRS wavefield attributes as

$$v_{NMO}^2 = \frac{2\,v_0\,R_{NIP}}{t_0\,\cos^2\alpha}\,. \tag{2}$$

The next two search steps are applied to the CMP stacked section. The search parameters are α and R_N. The former is then used to calculate R_{NIP} by means of formula (2).

Conflicting dips. This three-step strategy has to be modified if conflicting dips are to be correctly taken into account. Unfortunately, in spite of the angle-dependence of v_{NMO}, I cannot rely on the first step to separate events with different emergence angles because the associated stacking velocities might be similar or even identical. Furthermore, the sign of the emergence angle α cannot be determined by means of Equation (2).
However, it is possible to detect events with different emergence angles in the second step in the CMP stacked section, although these have not been correctly taken into account by the preceeding automatic CMP stack. This is indicated by Figure 1: for a given point in the ZO section to be simulated the coherency values are plotted versus the tested emergence angles. I observe three distinct local maxima which are potential candidates for conflicting dips.
Due to the above observations, the three-step approach can be easily extended such as to detect conflicting events with different emergence angles. However, the calculation of R_{NIP} from α and v_{NMO} according to Equation (2) is no longer possible because, in general, I will detect more than one angle of emergence but only one value for the stacking velocity v_{NMO}. Consequently, the approach has to be adapted to account for this fact. An additional search procedure for each radius of curvature $R_{NIP}^{(i)}$ corresponding to each conflicting dip $\alpha^{(i)}$ becomes necessary.
Unfortunately, $R_{NIP}^{(i)}$ can be determined neither in the CMP stacked section nor in the original CMP gathers. According to the stacking operator (1), $R_{NIP}^{(i)}$ has no influence in the ZO section ($h = 0$), and in the CMP

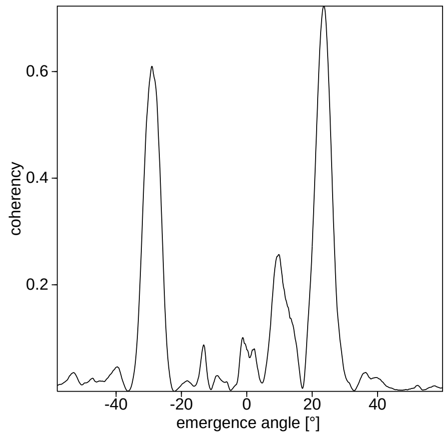

Figure 1: Coherency measure plotted versus the tested angles of emergence of the normal ray. Distinct local maxima can be observed, although conflicting dips have not been considered in the preceeding step. At the considered ZO location, two diffraction patterns (at $\alpha \approx -30°$ and $\alpha \approx 25°$, respectively) and a weak reflection event (at $\alpha \approx 12°$) intersect each other.

gather ($x_m = x_0$), $R_{NIP}^{(i)}$ and $\alpha^{(i)}$ cannot be separated. To solve this problem, I propose to perform the additional search for $R_{NIP}^{(i)}$ in another subset of the multi-coverage data, namely in the common-shot/common-receiver gather where $h^2 \approx (x_m - x_0)^2$. The simplified flowchart of this extended strategy reads:

$$\begin{array}{c}
\boxed{\text{multi-coverage data}} \\
\Downarrow \\
\boxed{\text{automatic CMP stack}} \\
\Downarrow \ \text{ZO section} \\
\boxed{\text{searches for } \alpha^{(i)} \text{ and } R_N^{(i)}} \\
\Downarrow \ \alpha^{(i)} \text{ and } R_N^{(i)} \\
\boxed{\text{search for } R_{NIP}^{(i)} \text{ in common-shot/common-receiver gather}} \\
\Downarrow \ \alpha^{(i)}, R_{NIP}^{(i)}, \text{ and } R_N{}^{(i)} \\
\boxed{\text{optional optimization and stack in multi-coverage data}}
\end{array}$$

First results. Details of the results obtained with the extended CRS stack for marine data are shown in Figure 2. The multitude of resulting wavefield attribute sections is far beyond the scope of this abstract, thus only the final stack result and the emergence angle sections for the first two conflicting events are shown.
The steep event in the center of the figures intersects several other events. At the intersection points, at least two different stacking operators (and their associated wavefield attributes) have been determined. This can been seen best in Figure 2b where the difference of the emergence angles for the first two conflicting events is depicted.
The outlined algorithm always determines a discrete number of conflicting events for each particular ZO location. For this purpose, the angle spectra (similar to the example shown in Figure 1) for each ZO location are analyzed applying user-given absolute and relative coherence thresholds.

Conclusions. The pragmatic approach of Müller (1998) to perform a ZO simulation by means of the CRS stack method can be adapted to also account for the conflicting dip problem. An additional one-parametric search is required to resolve ambiguities introduced by different events contributing to one and the same ZO sample to be simulated. The first results illustrate the applicability of this approach.
In addition to the more realistic simulated ZO section, the adapted CRS stack strategy provides three kinematic wavefield attributes for each particular event, even if it intersects one or more other events. Subsequent applications of these wavefield attributes (e. g., an inversion of the macro-velocity model, calculation of Fresnel zones etc.) benefit from this fact, because otherwise the wavefield attributes in the gaps between "broken" event segments would have to be interpolated.

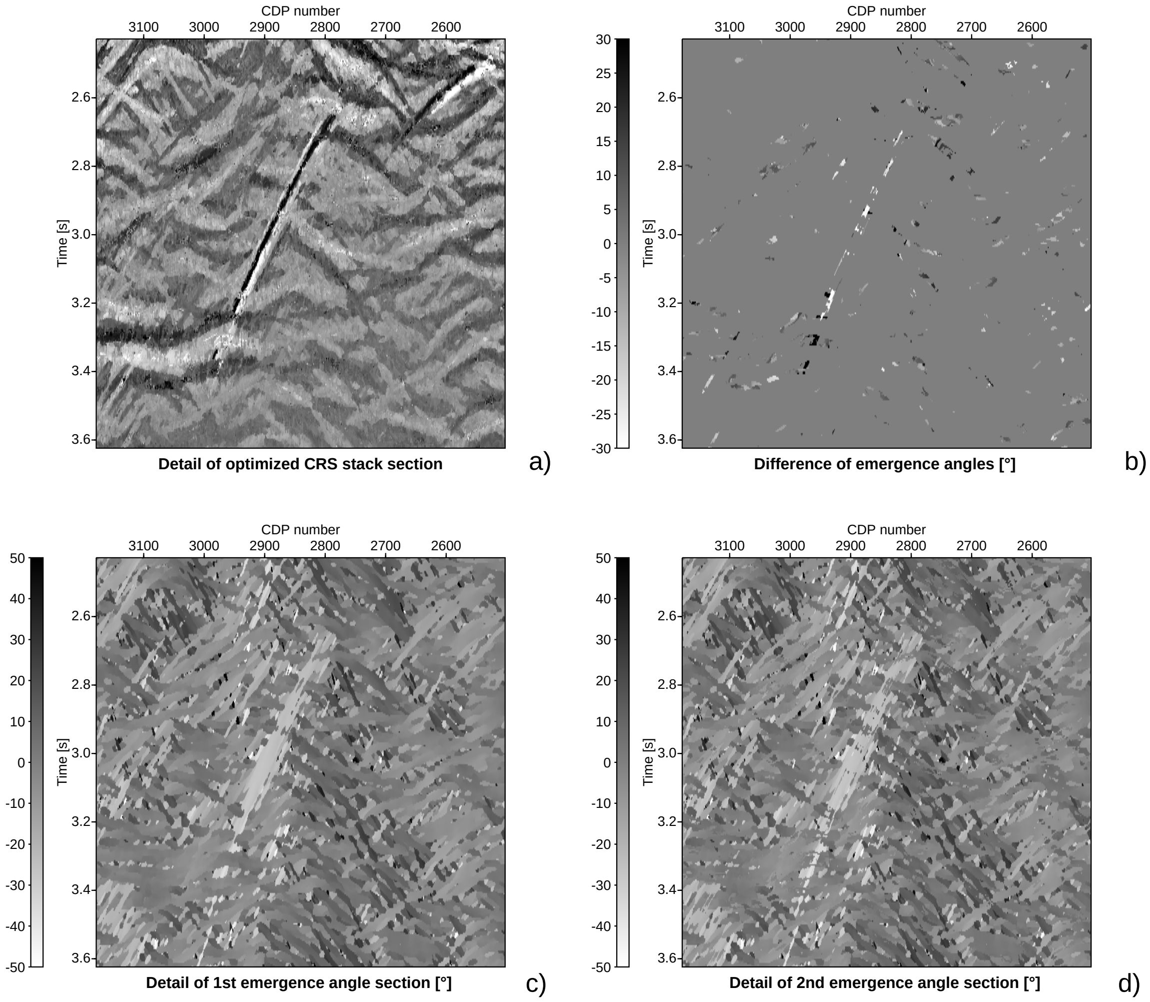

Figure 2: Details of the CRS stack results: a) optimized CRS stack section, c) and d) emergence angles of the first and second detected contributing events, b) difference of the emergence angles shown in c) and d).

Acknowledgments. This work was kindly supported by the sponsors of the *Wave Inversion Technology Consortium*, Karlsruhe, Germany and the *Federal Institute for Geosciences and Natural Resources*, Hannover, Germany.

References

Mann, J., Jäger, R., Müller, T., Höcht, G., and Hubral, P. (1999). Common-reflection-surface stack - a real data example. *J. Appl. Geoph.*, 42(3,4):301–318.

Müller, T. (1998). Common Reflection Surface Stack versus NMO/STACK and NMO/DMO/STACK. 60th Mtg. Eur. Assoc. Expl. Geophys., Extended Abstracts. Session 1-20.

Müller, T. (1999). *The common reflection surface stack - seismic imaging without explicit knowledge of the velocity model*. Der Andere Verlag, Bad Iburg.

Schleicher, J., Tygel, M., and Hubral, P. (1993). Parabolic and hyperbolic paraxial two-point traveltimes in 3D media. *Geophys. Prosp.*, 41(4):495–514.

Tygel, M., Müller, T., Hubral, P., and Schleicher, J. (1997). Eigenwave based multiparameter traveltime expansions. 67th Annual Internat. Mtg., Soc. Expl. Geophys., Expanded Abstracts, pages 1770–1773.